ISSN 0036-0244, Russian Journal of Physical Chemistry A, 2017, Vol. 91, No. 10, pp. 1883–1889. © Pleiades Publishing, Ltd., 2017.

CHEMICAL KINETICS AND CATALYSIS

Synthesis and Catalytic Performance of ZSM-5/MCM-41 Composite Molecular Sieve from Palygorskite[1]

Jinlong Jiang[a,b,*], Mei Wu[a], Yong Yang[a], Chuansong Duanmu[b], Jing Chen[a], and Xu Gu[b]

[a] *Faculty of Chemical Engineering, Key Laboratory for Palygorskite Science and Applied Technology of Jiangsu Province, Huaiyin Institute of Technology, Huaian 223003, P.R. China*

[b] *Jiangsu Provincial Engineering Laboratory for Advanced Materials of Salt Chemical Industry, Huaiyin Institute of Technology, Huaian 223003, P.R. China*

**e-mail: jiangjinlong75@163.com*

Received May 31, 2016

Abstract—ZSM-5/MCM-41 composite molecular sieve has been hydrothermally synthesized through a two-step crystallization process using palygorskite (PAL) as silicon and aluminum source. The products were characterized by various means and their catalytic properties for acetalization of cyclohexanone and esterification of acetic acid and *n*-butanol were also investigated. In the first step ZSM-5 zeolite could be formed from the acid-treated PAL after hydrothermal treatment using tetrapropylammonium bromide as template. XRD patterns, N_2 adsorption and desorption data, and TEM images show that the composite obtained in the secondary step had a well-ordered mesoporous MCM-41 phase and a microporous ZSM-5 zeolite phase. Compared with ZSM-5, ZSM-5/MCM-41 composite possessed more total acid amount, weak acid sites and large pore structure due to the formation of MCM-41 and exhibited higher catalytic activity for the acetalization and esterification reaction.

Keywords: palygorskite, ZSM-5, MCM-41, composite molecular sieve

DOI: 10.1134/S003602441710017X

1. INTRODUCTION

Zeolites are crystalline materials with uniform and ordered micropores and have been applied in petrochemical industry for their strong acidity and high hydrothermal stability. This microporous structure exhibited a high surface area and shape selectivity, but also limited the catalytic properties because of a low diffusion rate of reactants, especially in the reactions involving large molecules [1]. As compared to zeolites, composite molecular sieves with micro/mesoporous structure showed higher catalytic performance due to the synergistic effects of zeolitic and mesoporous phases in the reactions [2]. The micro/mesoporous composite materials have larger pore size, strong acidity of zeolites and integration of microporous and mesoporous structures, which avoided the restrictions of zeolites and enhanced the access for large molecules to the effective active sites, resulting in higher catalytic activity than that of mechanical mixture and individual molecular sieves [3, 4].

Several synthesis strategies were developed to prepare those composite materials such as co-synthesis, in situ and ex situ coating, and recrystallization of ordered mesoporous materials and zeolites by using different silicon sources [2]. For example, MFI/MCM-41 and MCM-49/ZSM-35 composite materials were one-step synthesized in the two-template synthesis gel system using sodium silicate [5] and silica sol [6] as silicon sources, respectively. Through a two-step crystallization process, namely an in situ coating method, ZSM-5/MCM-41, ZSM-5/MCM-48, Beta/MCM-41, and MCM-22/MCM-41 composite materials were also synthesized with two templates from different silicon sources such as fume silica [4, 7], sodium silicate [3, 8], silica sol [9], and tetraethoxysilane [10]. In the ex situ coating method, the preformed zeolite seeds [11] and zeolite crystals [12, 13] were added into the mesoporous molecular sieve synthesis gel prepared from tetraethoxysilane, resulting in the formation of Beta/MCM-41 and Y/MCM-48 composite after hydrothermal treatment. In addition, MOR/MCM-41, ZSM-5/MCM-41, and ZSM-5/SBA-15 were also obtained through recrystallization of zeolites [14–17], ion-exchanged TPA-mesoporous materials [18], and SBA-15 [19] in the alkaline solution, respectively. To avoid using expensive chemicals and environmental contamination, a clay mineral, kaolin, was used to prepare micro/mesoporous composite materials such as kaolin/NaY/MCM-41 and Ln-ZSM-5/MCM-41 composites [20, 21].

[1] The article is published in the original.

Palygorskite (PAL) is also a clay mineral and has been used as catalyst carrier, adsorbent, desiccant and polymer filler. In the last few years, there have a few reports that PAL was in situ converted to MCM-41 [22], zeolite A [23], and ZSM-5 [24, 25] after mechanical grinding and acid treatment or acid leaching, followed by hydrothermal treatment. The latter showed high catalytic cracking performance for Canadian light gas oil [24].

In this study, ZSM-5/MCM-41 composite molecular sieve was prepared from cheap PAL as silicon and alumina source through a two-step crystallization process. The products prepared in different crystallization stage were characterized by using various means and tested in the acetalization of cyclohexanone and esterification of acetic acid and *n*-butanol.

2. EXPERIMENTAL

2.1. Synthesis of ZSM-5/MCM-41

PAL was pretreated according to the published procedure [23] in an HCl solution (3 mol/L) at 80°C for 48 h. In a typical synthesis, 3 g of acid-treated PAL was added into 20 mL of NaOH solution (1 mol/L) and magnetically stirred for 30 min. A solution containing 20 mL of H_2O and 0.4 g of tetrapropylammonium bromide (TPABr) was then slowly dropped into the PAL solution, which was further stirred at room temperature for 24 h. The resultant mixture was heated to 180°C in a stainless steel autoclave with Teflon liner and kept for 48 h. Then, 0.4 g of NaOH was added into the colloidal mixture under magnetic stirring after the autoclave was cooled down to room temperature. After 1-h stirring, 20 mL of cetyltrimethylammonium bromide (CTAB) solution (10%) was added into the mixture and the pH value was adjusted to 10–11 with a diluted HCl solution (1 mol/L). The chemical composition of the acid-treated PAL was as follows: 0.04% Na_2O, 2.17% Al_2O_3, 80.66% SiO_2, 0.55% K_2O, 0.01% CaO, 0.01% MnO_2, 0.8% TiO_2, 0.21% Fe_2O_3, and 0.18% MgO [23]. Thus, the molar composition of the synthesis gel was 3 TPABr : 80.6 SiO_2 : 1.36 Al_2O_3 : 11 CTAB : 30 Na_2O : 6666 H_2O. Subsequently, the mixture was again heated at 100°C for 96 h after 1-h aging. Finally, the solid product was filtered, washed with deionized water, and dried at 100°C for 24 h. The organic templates were removed by calcination at 550°C for 3 h. For comparison, ZSM-5 zeolite could be obtained from the mixture prepared by hydrothermal treatment at 180°C for 48 h.

The products were ion-exchanged with 0.2 mol/L NH_4NO_3 solution at 80°C for 2 h. Then the ion-exchanged products were filtered and dried. The above procedure was repeated two times and H-form catalysts were then obtained by calcining NH_4^+-form molecular sieve at 550°C for 3 h.

2.2. Characterization

XRD patterns of the samples were collected on a D8 Discover X-ray powder diffractometer (Bruker) using CuK_α radiation (40 kV, 40 mA). Scanning electron microscopy (SEM) images and element analysis of the samples were obtained by using the Hitachi S-3000N microscope with integrated energy dispersive X-ray analytical system (EDX, Horiba EX-250). Transmission electron microscopy (TEM) micrographs were determined on a JEM 2010 with an accelerating voltage of 200 kV. The N_2 adsorption-desorption isotherms and textural properties of the samples were recorded with a Micromeritics TriStar II 3020 at 77 K. The samples were outgassed at 300°C for 3 h in N_2 atmosphere before the measurements. The total surface area (S_{BET}) was calculated by the standard BET method. The total pore volume (V_{tot}) was calculated from the desorption branch of the isotherm at $P/P_0 = 0.99$, assuming complete pore saturation. The micropore volume (V_{micro}) and micropore surface area (S_{micro}) were evaluated by the t-plot method. Mesopore volume (V_{meso}) was calculated by subtracting micropore volume from total volume. FT-IR spectra of the samples were collected on a Nicolet 5700 spectrometer with a resolution of 4 cm^{-1}. Temperature programmed desorption of ammonia (NH_3-TPD) was performed on a Quantachrome Chembet Pulsar TPR/TPD instrument equipped with a thermal conductivity detection (TCD). The samples (0.1 g) were pretreated at 500°C for 2 h and then cooled down to 100°C under flowing He. A mixture of 8% NH_3 in He was then introduced to be adsorbed onto the samples for 30 min. To remove the physical adsorbed NH_3, the He stream was passed the samples at the same temperature until no more NH_3 was observed in the exit flow. The samples were then heated at 600°C at a heating rate of 10°C/min to release NH_3 and the amount of desorbed ammonia was determined by TCD.

2.3. Catalytic Evaluation

2.3.1. Acetalization of cyclohexanone. The acetalization reaction of cyclohexanone with methyl alcohol was carried out in a round-bottom flask equipped with a condenser and magnetic stirring. The catalytic reaction was performed according to the procedure and condition in the literature [26]. The catalyst (H^+ form, 50 mg) was added into a solution containing of 10 mL methyl alcohol and 98 mg of cyclohexanone. After the reaction mixture was stirred at 50°C for 4 h, the reaction liquid was separated by centrifugation and analyzed by an Agilent 6820 gas chromatograph with a DB-1 column. The butyl acetate was used as an internal standard.

2.3.2. Esterification of acetic acid and *n*-butanol. A typical esterification of acetic acid and *n*-butanol was carried out as follows: 100 mg of catalyst, 4.77 mL

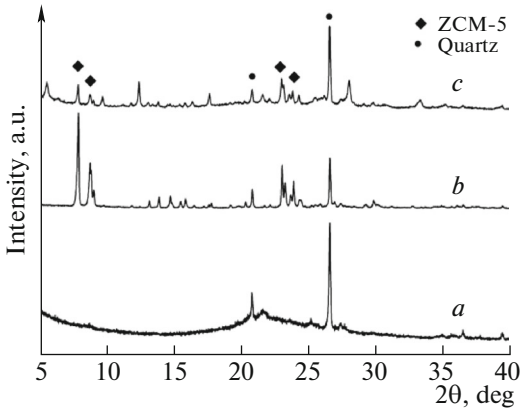

Fig. 1. Wide-angle XRD patterns of the acid-treated PAL (*a*), the product obtained in the first step (*b*), and the final product (*c*).

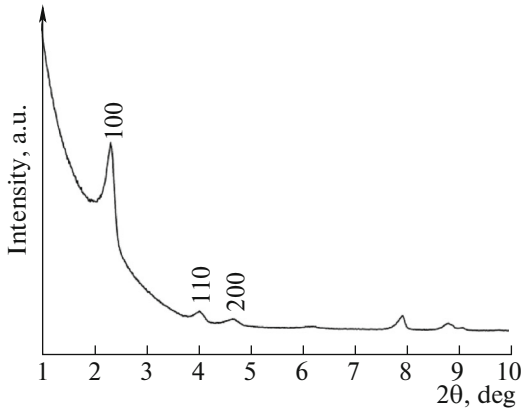

Fig. 2. Small-angle XRD pattern of the final product.

of acetic acid (83.3 mmol), 8.4 mL of *n*-butanol (91.7 mmol) were added to a three flask equipped with a reflux condenser and a mechanical agitator. The reaction mixture was stirred at 120°C for 120 min. The catalyst was separated from the resulting mixture by centrifugation. The product was analyzed by an Agilent 6820 gas chromatograph with a HP-INNO WAX column. The cyclohexanone was used as an internal standard.

3. RESULTS AND DISCUSSION

3.1. Characterization of ZSM-5/MCM-41

3.1.1. XRD and EDX analysis. Figure 1 shows the wide-angle XRD patterns of the acid-treated PAL and the products synthesized in different crystallization stage. The characteristic peaks of PAL at 2θ range of 8°–10° disappeared after treatment in hot HCl solution [27]. PAL was converted into amorphous silica and the acid-treated PAL could be used as silicon source for the synthesis of molecular sieves [23]. The diffraction peaks located at 2θ = 7.9°, 8.7°, 23.1°, 23.9°, and 24.4°, ascribed to the characteristic diffraction peaks of MFI-type zeolite structure [28], appeared in the XRD curves of two products. Those results indicate that MFI-type zeolites (ZSM-5 zeolites) were obtained from the acid-treated PAL by using TPABr as template after hydrothermal treatment at 180°C for 48 h [25]. The diffraction peaks of ZSM-5 zeolites remained in the final product and its intensity became weaker after recrystallization of the mixture obtained in the first crystallization stage by adding CTAB as template. The results demonstrate that partial ZSM-5 zeolite crystals might be destroyed in the alkali solution at the secondary crystallization stage and used as silicon source of molecular sieve [15, 16]. It is noted that the diffraction peaks of quartz from raw material still existed in the final product because of the stability of quartz for acid and alkali solution.

The small-angle XRD pattern of the final product is displayed in Fig. 2. Three distinct diffraction peaks (100), (110), and (200) appeared in the XRD curve, which demonstrates the presence of the hexagonally ordered MCM-41 mesoporous structure [22]. From the small-angle and wide-angle XRD analysis of the final product, ZSM-5/MCM-41 composite molecular sieve with micro/mesoporous structure was successfully synthesized from the acid-treated PAL through a two-step crystallization process.

The Si/Al ratio of the molecular sieve is an important parameter related with the catalytic properties of the molecular sieve catalyst. Our latest studies revealed that Al atoms in PAL could enter into the internal framework of the synthesized zeolite and the Si/Al molar ratio of ZSM-5 zeolite crystal was 92 [25]. Figure 3 shows the EDX analysis of two samples. It can be seen that aluminum and silicon elements could be observed in the EDX spectrometry of two samples. The corresponding Si/Al ratio of ZSM-5 and ZSM-5/MCM-41 composite was 11.65 and 7.57, respectively. Due to the leaching of silicon element in the alkali solution, the Si/Al ratios of both products were higher than that of the acid-treated PAL (32.76) [23] and the Si/Al ratio of the product decreased with the increase of the alkali treatment cycle. The results indicate that ZSM-5/MCM-41 composite possessed higher aluminum content and may be beneficial to improve the catalytic properties of catalyst [26].

3.1.2. SEM and TEM analysis. Figure 4 shows the SEM images of the products synthesized in different crystallization stage. The acid-treated PAL remained the fiber morphology derived from PAL after acid treatment (the results not shown here) [23, 25]. The acid-treated PAL was continually dissolved in the alkali solution and provided the silicon nutrition for the growth of zeolite during the hydrothermal treatment process. Therefore, ZSM-5 zeolite obtained from fibrous acid-treated PAL in the first crystallization stage exhibited round shape or coffin shape and the particle size of crystals was about 4–6 μm. After

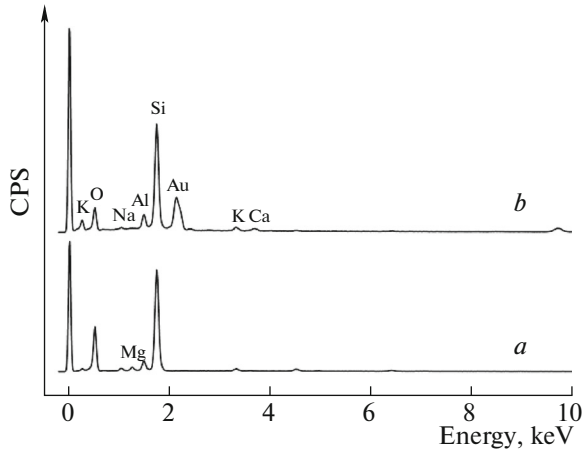

Fig. 3. Energy dispersive X-ray spectrometry of ZSM-5 (*a*) and ZSM-5/MCM-41 composite (*b*).

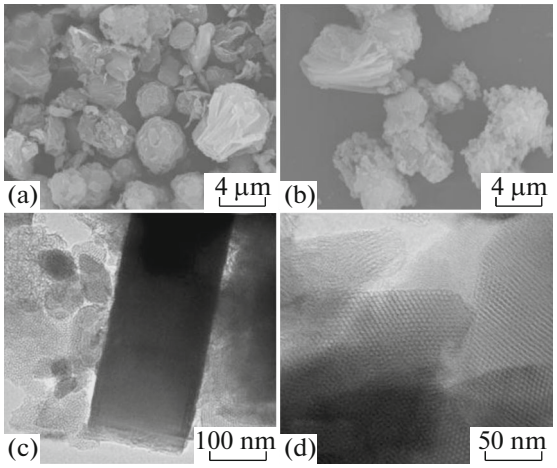

Fig. 4. SEM (a, b) and TEM (c, d) images of ZSM-5 (a) and ZSM-5/MCM-41 composite (b–d).

the secondary crystallization, the grain size of solid particles increased and irregular nano-sized particles appeared in the surface of ZSM-5 zeolite crystals. From the XRD analysis, the nano-sized particles were MCM-41 molecular sieve phase.

Figure 4 also displays the TEM images of ZSM-5/MCM-41 composite. After two-step crystallization process, the TEM image of the final product reveals that coffin shaped crystals were existed in the product, which is similar to the shape of ZSM-5 synthesized from the cupola slag appeared in the composite [29]. Combined with the XRD analysis result, the coffin shaped crystals can be identified as ZSM-5 zeolites. In addition, mesoporous framework of regular order hexagonal arrays, which confirmed the mesoporous MCM-41 structure [21], could be observed and firmly attached to the coffin-shaped ZSM-5 zeolite crystal. The results further confirm the formation of micro/mesoporous structure in the composite and indicate that mesoporous phase was in situ coated on the surface of ZSM-5 zeolite crystals in the process of hydrothermal treatment.

3.1.3. N_2 adsorption and desorption. Figure 5 shows the N_2 adsorption-desorption isotherms of the as-synthesized ZSM-5 and ZSM-5/MCM-41 composite. The as-synthesized ZSM-5 exhibited a representative type I isotherm according to the IUPAC classification, which was characteristic of microporous materials [16]. In contrast, the N_2 adsorption-desorption isotherm of ZSM-5/MCM-41 composite was typical of type IV, which was characteristic of MCM-41 mesoporous materials with one-dimensional cylindrical channels [21], and that indicated the existence of mesopores. A sharp inflection at P/P_0 = 0.3–0.4 was clearly observed in the ZSM-5/MCM-41 composite isotherm, which suggested uniformity of the mesopore channels. Furthermore, a hysteresis loop could be observed from the ZSM-5/MCM-41 composite isotherm at relative pressure above 0.9, which might be related to condensation in textural porosity [22]. The nitrogen adsorption of ZSM-5/MCM-41 composite was also significantly higher than that of ZSM-5. Table 1 shows the texture properties of ZSM-5 and ZSM-5/MCM-41 composite. Compared with the as-synthesized ZSM-5, ZSM-5/MCM-41 composite possessed higher specific surface area, total and mesopore volume, however, micropore surface area and volume of ZSM-5/MCM-41 composite decreased because of the partial destroy of ZSM-5 crystals in the alkali synthesis solution. The results indicate that the formation of MCM-41 in the composite could effectively increase specific surface area, total and mesopore volume, which may improve the adsorption and catalytic properties of the composite.

Table 1. Texture properties of ZSM-5 and ZSM-5/MCM-41 composite

Sample	S_{BET} (m^2/g)	S_{micro} (m^2/g)	V_{tot} (cm^3/g)	V_{micro} (cm^3/g)	V_{meso} (cm^3/g)
ZSM-5	266	124	0.149	0.057	0.092
ZSM-5/MCM-41	323	116	0.272	0.052	0.220

3.1.4. FT-IR spectra analysis. The IR spectra of the acid-treated PAL, ZSM-5, and ZSM-5/MCM-41 composite are shown in Fig. 6. Two bands at 796 and 1090 cm^{-1}, ascribed to the symmetrical and asymmetrical stretching vibration of Si–O–Si [23], respectively, appeared in all IR spectra of samples. The strong band at 454 cm^{-1} of ZSM-5 and ZSM-5/MCM-41 composite was due to the tetrahedral Si–O bending mode [21]. However, the band at 454 cm^{-1} of the acid-treated PAL was shifted to higher wave numbers. These features were characteristics of any silica-containing materials. Compared to the acid-treated PAL, there were two new bands at 546 and

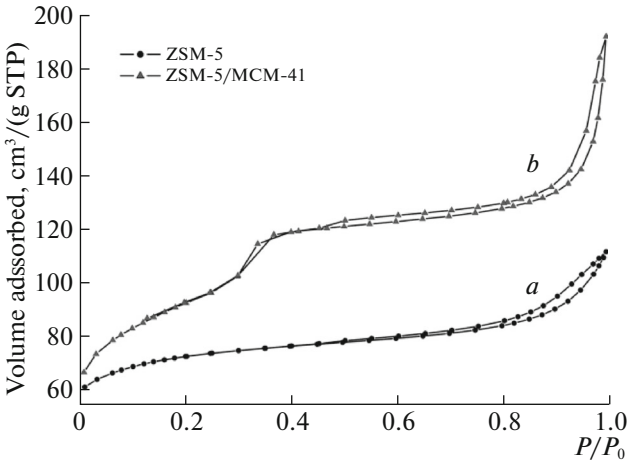

Fig. 5. N_2 adsorption-desorption isotherms of ZSM-5 (*a*) and ZSM-5/MCM-41 composite (*b*).

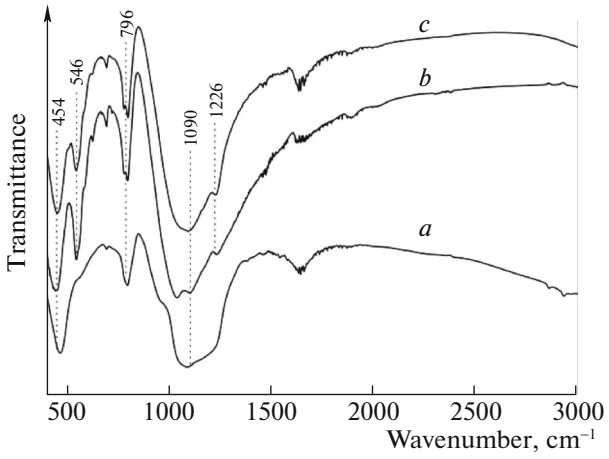

Fig. 6. FT-IR spectra of the acid-treated PAL (*a*), ZSM-5 (*b*), and ZSM-5/MCM-41 composite (*c*).

1226 cm^{-1} in the IR spectra of ZSM-5 and ZSM-5/MCM-41 composite, which were due to the double-rings tetrahedral vibration and antisymmetric stretching vibration of Si and AlO_4 tetrahedra in ZSM-5 zeolite framework [30], respectively.

3.1.5. NH_3-TPD analysis. Acid distributions of HZSM-5 and HZSM-5/MCM-41 composite were investigated by NH_3-TPD method. As shown in Fig. 7, two peaks appeared in the NH_3 desorption curves of all samples. Low temperature (100–350°C) desorption peak displayed weak adsorption acid sites, and the peak at high temperature (400–550°C) was ascribed to the interaction of NH_3 with strong acid sites [26]. It can be seen that the profile of HZSM-5/MCM-41 composite in high temperature range was similar to that of HZSM-5 and the strong acid sites were similar to that of HZSM-5. However, the amount of NH_3 desorbed from HZSM-5/MCM-41 composite in low temperature range was significantly higher than that of HZSM-5, revealing the higher concentration of weak acid sites in HZSM-5/MCM-41 composite and the presence of Al atoms in the MCM-41 mesoporous phase. The results also illustrate that Al species dissolved during alkali treatment of ZSM-5 [31] and PAL could incorporate into the framework of MCM-41 during recrystallization process. The corresponding acidic properties were shown in Table 2. It can be seen that the strong acid sites of HZSM-/MCM-41 composite (0.117 mmol/g) was slightly higher than that of HZSM-5 (0.101 mmol/g). However, its total acid amount and weak acid sites were remarkably higher than that of HZSM-5, which was caused by the introduction of MCM-41 molecular sieve and higher aluminum content of the composite. Compared with as-synthesized ZSM-5 zeolites, ZSM-5/MCM-41 composite may possess higher catalytic activity for the acid-catalytic reaction because of its stronger acid activity.

3.2. Catalytic Properties

Acetalization reaction of cyclohexanone with methanol was carried out to verify the catalytic activity of as-synthesized ZSM-5 and ZSM-5/MCM-41 composite. The results are listed in Table 3. The conversion yield of cyclohexanone on ZSM-5/MCM-41 composite reached to 87.07%, significantly higher than that of ZSM-5 (76.29%), close to that of mesoporous ZSM-5 (87.3%) and higher than commercial ZSM-5 (85.0%) at the same reaction conditions [26]. The latter mesoporous ZSM-5 and commercial ZSM-5 were prepared by using expensive tetraethoxysilane (TEOS) as silicon source and possessed smaller crystallite size (200–300 nm) [26]. The introduction of mesopores in the catalyst could effectively increase the conversion of cyclohexanone for favorable access of the reactants to the active sites [26, 32]. Na et al. [33] measured the pyridine and 2,4,6-trimethyl pyridine adsorbed IR spectra of ZSM-5 and ZSM-5/MCM-41 composite and their results indicated that ZSM-5/MCM-41 composite exhibited higher accessibility of acid sites compared to ZSM-5. Therefore, compared to ZSM-5, the high acid site accessibility and diffusivity of ZSM-5/MCM-41 composite resulted in higher catalytic performance for the acetalization reaction of cyclohexanone. In addition, the conversion yield of ZSM-5/MCM-41 composite was also higher than that of Al-MCM-41 (76.2%) for its strong

Table 2. Acidity properties of HZSM-5 and HZSM-5/MCM-41 composite

Sample	Acidity (mmol/g)		
	total acid amount	weak acid sites	strong acid sites
HZSM-5	0.747	0.646	0.101
HZSM-5/MCM-41	1.508	1.392	0.117

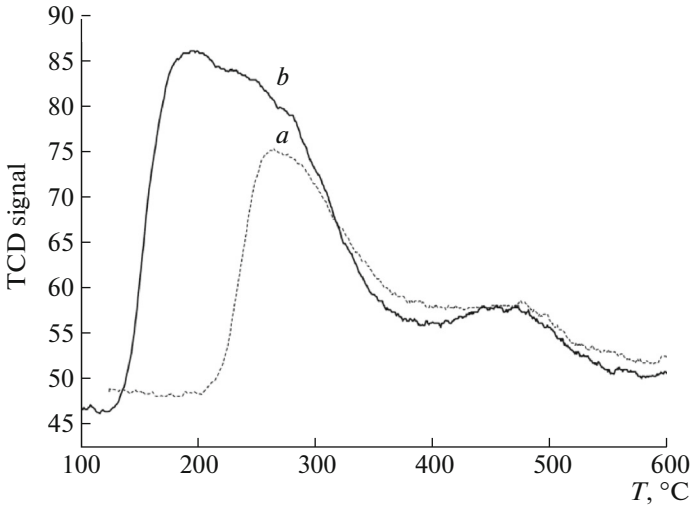

Fig. 7. NH_3-TPD of HZSM-5 (*a*) and HZSM-5/MCM-41 composite (*b*).

acid activity inherited from ZSM-5 zeolite [32]. On other hand, the selectivity of 1,1-dimethoxycyclohexane on ZSM-5/MCM-41 composite was 96.83% and similar to that of ZSM-5 (96.38%), also higher than that of mesoporous ZSM-5 and commercial ZSM-5 (ca. 92%) [26]. Similar selectivity of two products was attributed to the similar environment in zeolites for all aluminum atoms were 4-coordinate state in the ZSM-5 zeolite framework [26]. Thus, alkali treatment of ZSM-5 and then recrystallization process had no influence of the incorporation state of aluminum species in the zeolite framework. The same results were also found by Na and co-worker [33]. Those results illustrate that micro/mesoporous composite structure could effectively increase the catalytic activity of the composite because of the synergistic effects of zeolitic and mesoporous phases in the composite.

Table 3 also exhibits the conversion yield of acetic acid on different catalysts. The esterification reaction possessed good ester selectivity for the two catalysts. However, the conversion yield of acetic acid catalyzed by HZSM-5/MCM-41 composite was 75.52% and significantly higher than that of HZSM-5 (59.10%). The result is higher than the conversion of Al-MCM-41 with Si/Al molar ratio of 25 (60%) and HZSM-5 with Si/Al molar ratio of 15 (42.7%) [34, 35], indicating that the HZSM-5/MCM-41 composite possessed good catalytic property for the esterification reaction. In the esterification reaction, the acidity and pore structure properties of catalysts play a decisive role in the reaction conversion [36]. The esterification of acetic acid with *n*-butanol was primarily catalyzed by the weak and medium strength acidic sites when two catalysts possessed the similar nature [34, 35, 37]. Furthermore, the high surface area and large pore volume of the catalyst was beneficial to increasing its catalytic performance [37]. Thus, the high catalytic performance of HZSM-5/MCM-41 composite was derived from its high acid activity, the abundant weak acid sites and easy accessibility to acid sites compared to HZSM-5 and Al-MCM-41. The result suggests that ZSM-5/MCM-41 composite may have potential application in the esterification reaction.

4. CONCLUSIONS

In summary, ZSM-5/MCM-41 composite molecular sieve was successfully synthesized from low-cost PAL through a two-step crystallization process. In the first crystallization stage, ZSM-5 crystals were obtained from the acid-treated PAL by using TPABr as the template. Subsequently, the composite containing mesoporous MCM-41 and microporous ZSM-5 zeolite could be synthesized under hydrothermal condition after addition of NaOH and CTAB template. Due to the presence of MCM-41, the composite could

Table 3. Catalytic properties of HZSM-5 and HZSM-5/MCM-41 composite

Sample	Acetalization reaction		Esterification reaction	
	cyclohexanone conversion (%)	1,1-dimethoxycyclohexane selectivity (%)	acetic acid conversion (%)	ester selectivity (%)
HZSM-5	76.29	96.38	59.10	100
HZSM-5/MCM-41	87.07	96.83	75.52	100

improve the diffusion rate of reactants and possessed higher total acid amount and more weak acid sites compared to ZSM-5. As a result, the ZSM-5/MCM-41 composite exhibited higher catalytic activity for acetalization of cyclohexanone and esterification of acetic acid and *n*-butanol. The ZSM-5/MCM-41 composite molecular sieve synthesized from PAL with high acidity may be a potential catalyst for the esterification, alkylation, and condensation reaction, etc.

ACKNOWLEDGMENTS

This work was supported by the National Natural Science Foundation of China (51574130), State Key Laboratory of Materials-Oriented Chemical Engineering (no. KL14-14), Key Laboratory for Palygorskite Science and Applied Technology of Jiangsu Province (HPK201303), Qing Lan Project of Jiangsu Province and Jiangsu Provincial Engineering Laboratory for Advanced Materials of Salt Chemical Industry (SF201303).

REFERENCES

1. R. Chal, C. Gérardin, M. Bulut, and S. V. Donk, ChemCatChem **3**, 67 (2011).
2. I. I. Ivanova and E. E. Knyazeva, Chem. Soc. Rev. **42**, 3671 (2013).
3. D. K. Ji, S. Y. Li, F. C. Ding, and Y. L. Chi, Chin. Pet. Process Petrochem. Technol. **4**, 10 (2009).
4. Z. T. Zhang, Y. Han, F. S. Xiao, S. L. Qiu, L. Zhu, R. W. Wang, Y. Yu, Z. Zhang, B. S. Zou, Y. Q. Wang, H. P. Sun, D. Y. Zhao, and Y. Wei, J. Am. Chem. Soc. **123**, 5014 (2001).
5. A. Karlsson, M. Stöcker, and R. Schmidt, Microporous Mesoporous Mater. **27**, 181 (1999).
6. S. J. Xie, S. L. Liu, Y. Liu, X. J. Li, W. P. Zhang, and L. Y. Xu, Microporous Mesoporous Mater. **121**, 166 (2009).
7. W. P. Guo, L. M. Huang, P. Deng, Z. Y. Xue, and Q. Z. Li, Microporous Mesoporous Mater. **44–45,** 427 (2001).
8. L. M. Huang, W. P. Guo, P. Deng, Z. Y. Xue, and Q. Z. Li, J. Phys. Chem. B **104**, 2817 (2000).
9. M. Kollár, R. M. Mihályi, G. Pál-Borbély, and J. Valyon, Microporous Mesoporous Mater. **99**, 37 (2007).
10. C. He, J. J. Li, P. Li, J. Cheng, Z. P. Hao, and Z. P. Xu, Appl. Catal. B: Environ. **96**, 466 (2010).
11. P. Prokešová, N. Ďilková, S. Mintova, T. Bein, and J. Čejka, Appl. Catal. A: Gen. **28**, 85 (2005).
12. A. M. Alsobaai, R. Zakaria, and B. H. Hameed, Fuel Process. Technol. **88**, 921 (2007).
13. Z. F. Tao, Q. Zhao, Y. Ma, J. Jia, and T. S. Jiang, J. Chin. Ceram. Soc. **40**, 1466 (2012).
14. L. Wang, T. Dou, Y. P. Li, X. F. Li, and Z. C. Yan, Catal. Commun. **6**, 87 (2005).
15. C. M. Song, J. Jiang, and Z. F. Yan, J. Porous Mater. **15**, 205 (2008).
16. Q. Tang, H. Xu, Y. Y. Zheng, J. F. Wang, H. S. Li, and J. Zhang, Appl. Catal. A: Gen. **413–414**, 36 (2012).
17. H. S. Li, S. C. He, K. Ma, Q. Wu, Q. Z. Jiao, and K. N. Sun, Appl. Catal. A: Gen. **450**, 152 (2013).
18. K. R. Kloetstra, H. van Bekkum, and J. C. Jansen, Chem. Commun. **23**, 2281 (1997).
19. S. Habib, F. Launay, H. E. Zakhem, M. Mazaj, F. Guenneau, P. Beaunier, D. Brouri, N. N. Tušar, V. Kaučič, and A. Gédéon, Mater. Res. Bull. **48**, 1288 (2013).
20. H. T. Liu, X. J. Bao, W. S. Wei, and G. Shi, Microporous Mesoporous Mater. **66**, 117 (2003).
21. X. Li, B. S. Li, J. Q. Xu, Q. Wang, X. M. Pang, X. H. Guo, Z. Y. Zhou, and J. R. Piao, Appl. Clay Sci. **50**, 81 (2010).
22. H. M. Yang, A. D. Tang, J. Ouyang, M. Li, and S. Mann, J. Phys. Chem. B **114**, 2390 (2010).
23. J. L. Jiang, L. D. Feng, X. Gu, Y. H. Qian, Y. X. Gu, and C. S. Duanmu, Appl. Clay Sci. **55**, 108 (2012).
24. X. Z. Zhou, Y. Liu, X. J. Meng, B. J. Shen, and F. S. Xiao, Chin. J. Catal. **34**, 1504 (2013).
25. J. L. Jiang, C. S. Duanmu, Y. Yang, X. Gu, and J. Chen, Powder Technol. **251**, 9 (2014).
26. H. X. Tao, C. L. Li, J. W. Ren, Y. Q. Wang, and G. Z. Lu, J. Solid State Chem. **184**, 1820 (2011).
27. M. Suárez, L. V. Flores, M. A. Vicente, and J. M. Martín-Pozas, Appl. Clay Sci. **10**, 247 (1995).
28. B. Y. Liu, C. Li, X. Q. Ren, Y. Z. Tan, H. X. Xi, and Y. Qian, Chem. Eng. J. **210**, 96 (2012)
29. R. Anuwattana, K. J. Balkus, Jr., S. Asavapisit, and P. Khummongkol, Microporous Mesoporous Mater. **111**, 260 (2008).
30. K. Kordatos, S. Gavela, A. Ntziouni, K. N. Pistiolas, A. Kyritsi, and V. Kasselouri-Rigopoulou, Microporous Mesoporous Mater. **115**, 189 (2008).
31. M. Ogura, S. Y. Shinomiya, J. Tateno, Y. Nara, M. Nomura, E. Kikuchi, and M. Matsukata, Appl. Catal. A: Gen. **219**, 33 (2001).
32. B. Rabindran Jermy and A. Pandurangan, J. Mol. Catal. A: Chem. **256**, 184 (2006).
33. J. D. Na, G. Z. Liu, T. Y. Zhou, G. C. Ding, S. L. Hu, and L. Wang, Catal. Lett. **143**, 267 (2013).
34. B. Rabindran Jermy and A. Pandurangan, Appl. Catal. A: Gen. **288**, 25 (2005).
35. B. Rabindran Jermy and A. Pandurangan, J. Mol. Catal. A: Chem. **237**, 146 (2005).
36. L. X. Hou, X. J. Yin, N. B. Long, S. J. Yang, and R. F. Zhang, Chin. J. Inorg. Chem. **28**, 239 (2012).
37. H. Pan, J. X. Wang, L. Chen, G. H. Su, J. M. Cui, D. W. Meng, and X. L. Wu, Catal. Commun. **35**, 27 (2013).